JOURNAL OF GEOPHYSICAL RESEARCH, VOL. 106, NO. B8, PAGES 16,357–16,374, AUGUST 10, 2001

Elastohydrodynamic lubrication of faults

Emily E. Brodsky[1] and Hiroo Kanamori

Seismological Laboratory, California Institute of Technology, Pasadena, California, USA

Abstract. The heat flow paradox provides evidence that a dynamic weakening mechanism may be important in understanding fault friction and rupture. We present here a specific model for dynamic velocity weakening that uses the mechanics of well-studied industrial bearings to explain fault zone processes. An elevated fluid pressure is generated in a thin film of viscous fluid that is sheared between nearly parallel surface. This lubrication pressure supports part of the load, therefore reducing the normal stress and associated friction across the gap. The pressure also elastically deforms the wall rock. The model is parameterized using the Sommerfeld number, which is a measure of the lubrication pressure normalized by the lithostatic load. For typical values of the material properties, slip distance and velocity, the Sommerfeld number suggests that lubrication is an important process. If the lubrication length scales as the slip distance in an earthquake, the frictional stress during dynamically lubricated large earthquakes is 30% less than the friction with only hydrostatic pore pressure. Elastohydrodynamic lubrication also predicts a decrease in high-frequency (>1 Hz) radiation above a critical slip distance of a few meters. This prediction is well matched by the strong motion data from the 1999 Taiwan earthquake. The observed 2 orders of magnitude variation in scaled radiated energy between small ($M_w < 4$) and large earthquakes ($M_w > 6$) is also predicted by the lubrication model.

1. Introduction

Lubricated bearings are used in industrial applications to minimize the friction and wear between moving parts that carry heavy loads. Faults also appear to have low friction and relatively little wear when they slip with large normal stresses [*Lachenbruch and Sass*, 1980; *Hubbert and Rubey*, 1959]. Low fault friction is puzzling to seismologists because it is not consistent with laboratory-based models of rock friction [*Byerlee*, 1970]. Proposed explanations for the apparent reduction in friction in the natural system include melting [*Jeffreys*, 1942], acoustic fluidization [*Melosh*, 1979], fault opening [*Brune et al.*, 1993; *Ben-Zion and Andrews*, 1998], and high pore pressure [*Sibson*, 1973]. The most common explanation is the last one. Interstitial fluids partially support the load between the fault planes and therefore reduce frictional resistance. Models generally use either the static values of pore pressure for this purpose [*Hubbert and Rubey*, 1959; *Byerlee*, 1990] or the elevated pressures due to frictional heating [*Lachenbruch*, 1980]. Here we consider a previously undiscussed contribution to the pore pressure during faulting based on strictly mechanical lubrication by a viscous fluid.

We propose that faults operate in a way analogous to lubricated bearings. In a bearing the fluid pressure increases during motion [*Reynolds*, 1886]. As two uneven solid surfaces slide past each other, they strain the viscous fluid between them. The finite viscosity of the fluid resists the motion, and a high pressure gradient is formed. This pressure produces a normal stress that can help to support the load. Hydrodynamic lubrication works in two ways to reduce the total frictional stress. (1) In the fraction of the bearing or fault area lubricated by a continuous film, the shear stress is the viscous stress which is significantly below the solid-solid friction for fluids such as water, slurry, or mafic melt. (2) More importantly, the mechanically increased pore pressure reduces the effective stress on the solid-solid interfaces and therefore dynamically reduces the frictional stress during an earthquake.

In this study we develop a theory to quantitatively predict the observable effects of coseismic lubrication by a viscous fluid in a confined fault. We first review the fundamental physics and mathematical formulation of elastohydrodynamics. We then present the results from numerical experiments on model systems in order to build a general understanding of lubrication behavior. Scaling relationships are then explored to explain the numerical results, to qualitatively describe the frictional behavior, and to determine the dependency of

[1]Now at Department of Earth and Planetary Science, University of California Berkeley, Berkeley, California, USA.

Paper number 2001JB000430.
0148-0227/01/2001JB000430$09.00

lubrication pressure on faulting parameters. We then estimate the values of the model parameters and quantitatively assess the importance of lubrication for earthquakes. The theory is applied to three specific observations: heat flow, near-field strong motion spectra, and radiated energy. A single parameter set is then found that is able to provide self-consistent explanations for all three applications. At the end of the paper we discuss some of the limitations of the simplified theory presented here and suggest future modifications.

Throughout this work we envision a seismogenic fault as a bicontinuous system of solid matrix and fault fluid. The fault fluid flows around asperities in a nearly linear path as the area of the asperity contacts is much less than the total fault surface area (Figure 1). The flow is modeled as two-dimensional, and the deflection due to the asperities is neglected. We calculate the fluid pressure generated by this flow and consider its effect on reducing the load on the asperities. We do not consider interseismic processes here. Our model is only applicable to the behavior during a single slip event.

The fault fluid is formulated as generally as possible since the physical process described refers to any viscous fluid sheared between two rough surfaces. We favor identifying the fluid as a slurry of fine-grained fault gouge and aqueous fluid because geological evidence for such a material exists [e.g., *Otsuki*, 1999] and slurry viscosities are large enough to produce significant lubrication pressures. Other candidate fault fluids include aqueous fluid and frictional melt. The general theory presented here applies equally well to any viscous fluid, although the numerical results would need to be recomputed with the appropriate material properties.

2. Lubrication Theory

A quantitative understanding of hydrodynamic lubrication requires a brief review of the standard formulation of the motion of the fluid between two subparallel planes. The fluid motion is completely described by the full Navier-Stokes equation,

$$\rho\frac{D\mathbf{u}}{Dt} = -\nabla p + \eta\nabla^2\mathbf{u}, \tag{1}$$

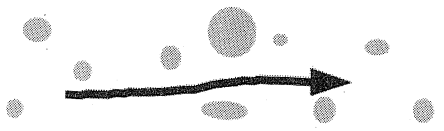

Figure 1. Map view of a fault surface. There is a bicontinuous system of solid matrix (rock) and fault fluid (slurry). The upper block (not shown) moves to the right relative to the lower block. The fluid is dragged around the asperities (shaded) in the nearly slip-parallel path direction shown by the arrow. Asperities comprise a small fraction of the fault surface but generate most of the friction.

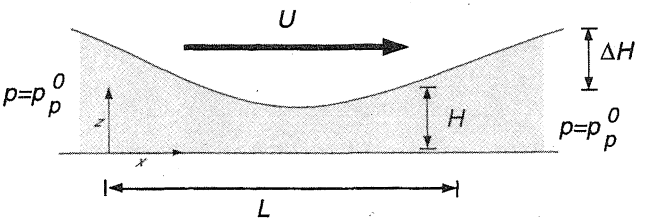

Figure 2. Characteristic dimensions H and L in a narrow fault. L is the characteristic dimension of pressure changes, and H is the mean height of the gap. Fluid is in the shaded area. For a fluid-filled fault the mean gap height is the same as the average thickness of the slipping zone. U is the slip velocity of one side of the fault relative to the other, p_p^0 is the undisturbed fluid pressure and ΔH is the average asperity height. All cartoons in this paper are vertically exaggerated.

where ρ is the density, $\mathbf{u}$ is the velocity vector, p is the pressure, and η is the viscosity. An important simplification of the Navier-Stokes equations can be made if the flow is through a thin gap, such as a fault zone. A thin gap is defined as one where the length L over which the fluid pressure changes significantly is much longer than the mean height H of the gap (Figure 2).

The thin gap simplification of the equations of motion is known as the lubrication approximation, and all terms in the Navier-Stokes equation of order H^2/L^2 or smaller are neglected. The inertial term is also negligible provided that the Reynolds number $Re \equiv \rho UH/\eta$ is much less than L/H, where U is the relative velocity between the fault surfaces [*Szeri*, 1998, p.72]. For faults during rupture both conditions are met and the governing equations in two dimensions reduce to

$$\frac{\partial p}{\partial x} = \eta\frac{\partial^2 u}{\partial z^2} \tag{2}$$

$$\frac{\partial p}{\partial z} = 0, \tag{3}$$

where u is the fluid velocity in the x direction and the adopted coordinate system defines x as parallel to the fault slip vector and z as the normal to the fault plane (Figure 2).

Pressure gradients across the gap are negligible under the above assumptions. The dynamics are dominated by the balance of the viscous stress and the dynamic pressure.

The continuity equation for an incompressible fluid is

$$\frac{\partial u}{\partial x} + \frac{\partial w}{\partial z} = 0 \tag{4}$$

where w is the velocity in the z direction. Combining (4) with the boundary conditions and the equations of motion (2) and (3) provides solutions for the velocity and pressure fields.

We adopt a frame of reference that is stationary at the wall where $z = 0$ and assume no slip boundary conditions at the walls:

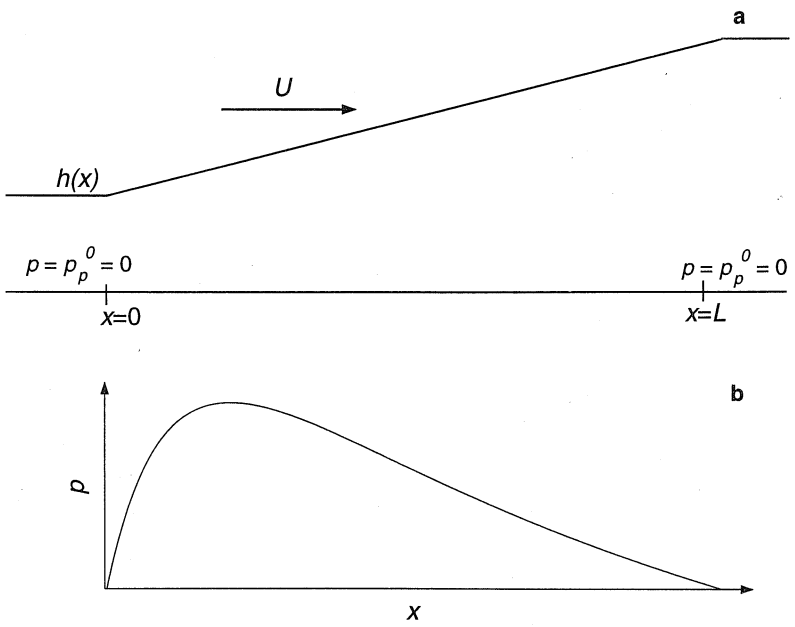

Figure 3. Lubrication under a tapered slider block. (a) A vertically exaggerated slider plate. (b) The pressure increase as calculated from (7) in arbitrary units.

$$\begin{aligned} &\text{At } z = 0, && u = 0, w = 0 \\ &\text{At } z = h, && u = U, w = 0. \end{aligned} \tag{5}$$

At the wall with $z = h$, where h is defined as the local slipping zone thickness, $u = U$ where U is the relative velocity between the fault walls. The relative motion between the walls is assumed to be entirely in the plane of the fault. The slipping zone height includes both the initial distance between the walls and any elastic displacement that may be caused by the fluid pressurization. At both walls ($z = 0$ and $z = h$), $w = 0$ since there is no flow in the direction normal to the impermeable walls.

We integrate (2), impose the boundary conditions (5), and use the integrated form of the continuity equation (4) to derive the Reynolds equation, a standard result in lubrication theory [e.g., *Hamrock*, 1994]:

$$\frac{d}{dx}\left(h^3 \frac{dp}{dx}\right) = -6\eta U \frac{dh}{dx}. \tag{6}$$

A more convenient integrated form is

$$p(x) - p_p^0 = 6\eta U \int_0^x \frac{h^* - h}{h^3} dx, \tag{7}$$

where h^* is the gap height at the point of maximum pressure, i.e., at $x = x^*$ where $dp/dx|_{x=x^*} = 0$. Given boundary conditions for p and the geometry of the fault specified by $h(x)$, the Reynolds equation can be solved to find the pressure distribution $p(x)$. The typical behavior of lubricated systems can be illustrated by considering a tapered slider moving over a plane surface (Figure 3).

The pressure in the far-field is the initial reservoir pressure p_p^0. It is convenient to reference all pressures to this level and to set p_p^0 equal to 0. The appropriate boundary conditions for pressure are that at $x = 0$ and $x = L$, the pressure $p = p_p^0 = 0$. The pressure rises in the narrow region and therefore exerts a net force or "lift" separating the two blocks.

3. Elastic Effects

To this point we have assumed that the fault wall behaves as a rigid body. This is not true in many lubrication problems. The fluid pressure deforms the wall and in so doing adjusts the geometry to make lubrication more effective. This phenomenon explains how originally symmetric asperities like that pictured in Figure 2 deform to generate a net pressure increase. The everyday experience that arbitrary rough surfaces slide more easily when lubricated than when dry is evidence of the efficacy of the elastic adjustment.

The lubrication pressure is significant as long as the fault is slipping. Since the asperities are at most a few meters long, the time it takes the elastic waves to traverse the asperities ($\ll 10^{-2}$ s) is likely much less than the duration of loading. Therefore a quasi-static solution to the elastic equations is likely to be appropriate for modeling the effect of lubrication pressure on the fault geometry. Additional processes, such as asperity collisions, simultaneously generate elastodynamic deformation (seismic waves) during rupture. Those dynamic effects are beyond the scope of the present study and may be superposed on the elastostatic solution presented here.

The elastostatic solution is derived in Appendix A for the displacement in a halfspace from a finite sheet of pressurized fluid. The elastic displacement at point x is

$$\delta(x) = \frac{4(1-\nu^2)}{\pi E} \int_0^L p(\xi) \ln \left| \frac{a+\sqrt{(x-\xi)^2+a^2}}{x-\xi} \right| d\xi \ , \qquad (8)$$

where $2a$ is the width of the lubricated zone in the fault plane direction normal to slip, E is the Young's modulus of the rock, and ν is the Poisson's ratio. We assume that the preearthquake pore pressure p_p^0 is in equilibrium with the initial asperity shape and produces no elastic displacement. Equation (8) is the solution for the displacement due to a finite sheet of pressure $p(x, y)$ with $\partial p/\partial y = 0$, where y is the slip normal direction in the fault plane (Appendix A). The elastic deformation is driven by the pressure distribution from the equation (7) which implicitly assumes that there is no flow in the y direction. Flow in the y direction could occur in the physical system if there is leakage from the ends of the slipping zone. For a lubricated zone that is much wider than long ($a \gg L$), the leakage is clearly negligible [*Hamrock*, 1994]. Leakage in the y direction may be a significant effect for narrower slipping zones. For now, we assume that the lubricated zone is equidimensional with $a = L/2$ in order to provide simple models of systems with a single asperity. This assumption will be modified to a condition that ensures $a \gg L$ when we consider rough surfaces rather than single asperities.

Figure 4 shows the deformation of an asperity with the initial shape $s(x) = h_1 [\cos(2\pi x/L) + 1] + h_0$, where the constants h_1 and h_0 are both 10^{-3} m for this example. Details of the numerical method are given in Appendix B. There are two features of the solution that are particularly important for the discussion that follows. (1) The asperity is deformed to an asymmetrical configuration, thus promoting lubrication and supporting a net load. (2) As the length L of the asperity increases, the displacement $\delta(x)$ increases in accordance with (8). Since the initial asperity height is the same in all three cases of Figure 4, the deformed asperity flattens with increasing values of L.

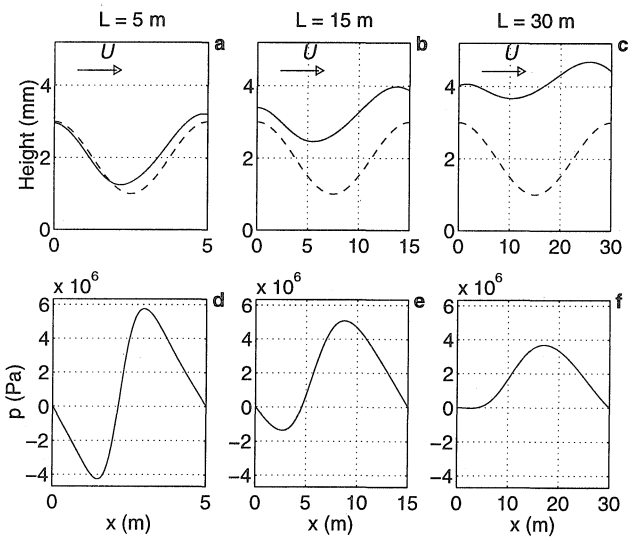

Figure 4. (a) Elastic deformation of a cosine asperity with an initial minimum separation of 1 mm and $L = 5$ m. The dashed line is the undeformed asperity shape $s(x)$ and the solid line is the equilibrium shape $h(x) = s(x) + \delta(x)$ with the elastic deformation coupled to the lubrication fluid pressure. Other parameters are $E = 5 \times 10^{10}$ Pa, $U = 1$ m/s, and $\eta = 10$ Pa s. (b) The same as Figure 4a with $L = 15$ m. (c) The same as Figure 4a with $L = 30$ m. (d) The change in pressure in the fluid due to lubrication effects with $L = 5$ m. The total change in gap height is plotted and includes the elastic displacement of both sides of the faults. (e) Same as Figure 4d with $L = 15$ m. (f) Same as Figure 4d with $L = 30$ m.

4. Rough Surfaces

The length of the lubricated zone L is defined as the length over which the pressure returns to its reservoir value. For a single asperity, such as shown in Figure 4, this is clearly the asperity length. Similarly, the asperity height ΔH is clearly defined for a single asperity (Figure 2). Real fault surfaces are observed to be self-similar and have asperities over a continuous range of lengths [*Scholz*, 1990; *Power and Tullis*, 1991]. Therefore it is necessary to derive the appropriate asperity length L and height ΔH for a rough lubricated surface.

Power and Tullis [1991] and *Brown and Scholz* [1985] measured fault surfaces on scales from 10^{-5}–40 m and found that the power spectrum followed power laws such as

$$G(f) \propto \frac{1}{f^\alpha}, \qquad (9)$$

where $G(f)$ is the power spectral density, f is the spatial frequency and the value of the exponent α is typically 2 or 3. For instance, the Fourier spectral density for a surface with a finite length $\mathcal{L}$ and $\alpha = 2$ is

$$\hat{g}(f) = \frac{K\mathcal{L}}{2f}, \qquad (10)$$

where K is the spectral aspect ratio. The corresponding surface roughness function is

$$g(x) = 2 \int_0^\infty \hat{g}(f) \cos(2\pi f x + \phi(f))\, df, \qquad (11)$$

where $\phi(f)$ is a random phase that varies with spatial frequency.

We assume that the shape of the two rough sides of the fault is initially well matched before the earthquake due to interseismic healing. The gap height $h(x)$ has a constant value h_0 along strike. If the fault fluid is a slurry, the thickness of this initially uniform fluid layer is controlled by the fluidization process as well as the fault surface geometry. The surface is "well matched" if the fluid layer is initially of uniform thickness on scales less than or equal to the final slip distance. As one side of the fault slips relative to the other, a mismatch between the fault sides develops and $h(x)$ varies with x (Figure 5):

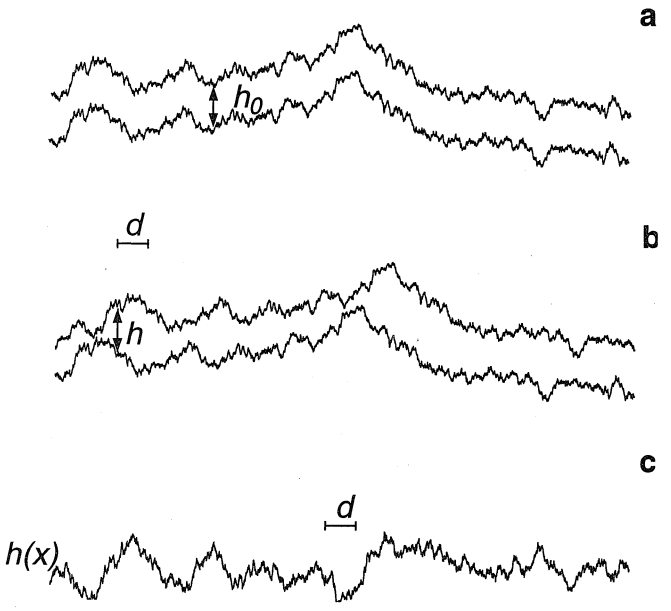

Figure 5. Roughness generated by slip on a self-similar surface. The rough surface is generated by the function $g(x)$ in equation (11). (a) Well-matched surfaces with a uniform layer thickness h_0 at the initiation of the earthquake. (b) Surfaces after the top surface slips a distance d relative to the bottom one. (c) The gap height function $h(x)$ after slip. The characteristic wavelength is comparable to the scale bar of length d. Surface roughness is vertically exaggerated.

$$h(x) = g(x + d) - g(x) + h_0. \tag{12}$$

If the initial roughness $g(x)$ is self-similar as assumed here, the characteristic wavelength of $h(x)$ scales approximately as the displacement between the two fault surfaces. This occurs because displacing the surfaces as in (12) is equivalent to passing $g(x)$ through a filter with the amplitude response of $\sin \pi f d$. Figure 5 shows how initially conformal, rough surfaces result in a high-frequency gap height function $h(x)$ when one plane is slipped a distance d relative to the other plane. Larger asperities are isolated with increasing displacement. Visual inspection suggests that d is the dominant asperity length and can be used as L.

The gap function theoretically has relatively large components at long wavelengths up to $\mathcal{L}$ because of the f^{-1} spectral density structure. For wavelength components where the spectral amplitude is much larger than the average gap height, at some points the two surfaces may collide. At other places they may be distant. Lubrication is only important where the separation is small. Therefore, if the theoretical spectrum holds to all wavelengths, only patches of the fault are hydrodynamically lubricated. However, it is unlikely that large wavelength asperities can be maintained during slip on a thin fault in the presence of collisions and elastic deformation. In any case, the elevated fluid pressure in lubricated patches reduces the average normal stress carried on contacting asperities across the fault. The scale of these lubricated regions is uncertain. The roughness data only extend to 40 m wavelengths, so it is difficult to extrapolate the behavior over any longer distance. If we use observational data on fault roughness from *Power and Tullis* [1991], at wavelengths $\gg$ 10 m asperity heights are greater than the value of total gap height (initial uniform height plus elastic displacement) used in this paper. Therefore we will assume that the lubricated regions are tens of meters long. Many discontinuous patches are postulated to exist in the slipping fault. Within these lubricated patches the gap function can be locally approximated by a sinusoidal wave with wavelength d and amplitude Kd. We use this simple monochromatic model with $L \approx d$ and $\Delta H \approx Kd$ to scale the lubrication pressure. It is likely that the result can apply generally to any self-similar fault surface that has a relatively uniform layer of fluid at the beginning of the earthquake.

Figure 6 is a calculation of elastohydrodynamic lubrication using a rough surface generated by (11). The gap height function is produced by slipping this surface a distance d relative to a well-matched surface as in (12). The increase in elastic displacement with increasing d reproduces the behavior shown in Figure 4 for a single asperity with increasing L. The separation between the original and deformed surfaces increases with d. An additional complication in the rough surface calculations is that the initial asperity height also increases with increasing d. Larger asperities become prominent in the gap height function as the slip distance increases since $\Delta H = Kd$. Therefore the flatten-

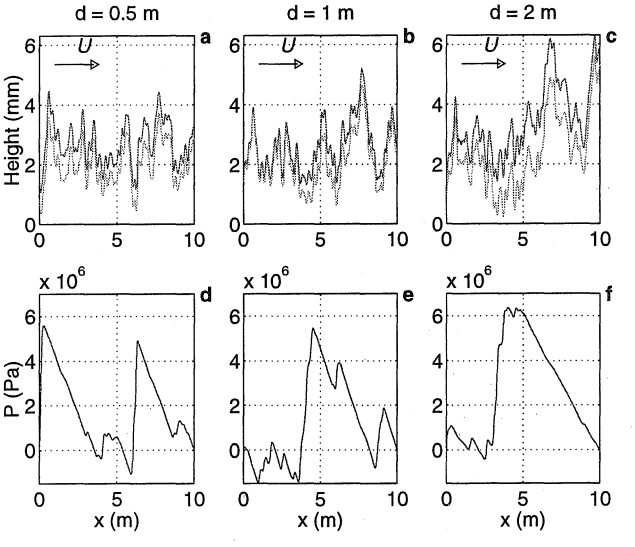

Figure 6. (a) Lubrication of a rough surface. The light curve is the undeformed asperity shape, and the heavy curve is the equilibrium shape. Parameters are as in Table 1 except $d = 0.5$ m and $K = 10^{-4}$. (b) The same as Figure 6a with $d = 1$ m. (c) The same as Figure 6a with $d = 2$ m. (d) The change in pressure in the fluid due to lubrication effects with $d = 0.5$ m. (e) Same as Figure 6d with $d = 1$ m. (f) Same as Figure 6d with $d = 2$ m.

ing is not apparent as in Figure 4. If d exceeds a critical value L_c, the gap is widened by an amount comparable to the largest asperity heights. The wider gap reduces the number of asperity collisions during sliding. It will be hypothesized that this process has observable effects in near-field strong motion records.

5. Scaling and the Sommerfeld Number

In the above discussion we have presented the basic theory of elastohydrodynamic lubrication and some numerical results. Now we will explore the scaling relationships between the lubrication pressure and the fault parameters. The scaling relationships both describe the qualitative behavior of the system and provide the basis for quantitative application of the theory.

Equation (6) balances the dynamic pressure in the gap with the viscous stresses generated by the variations in gap height and implies that the excess pressure due to lubrication, $P_L \equiv \mathcal{O}(p(x) - p_p^0)$, scales as

$$P_L \sim \frac{6\eta U L \Delta H}{H^3}, \tag{13}$$

where H is the mean gap height and $\Delta H \equiv \mathcal{O}(h - h^*)$ is the mean variation in gap height caused by asperities (Figure 2). Capital letters are used here to denote characteristic scales, while variables are in lowercase letters. The lubrication pressure increases with viscosity. This dependence on viscosity is why oil is a better lubricant than water for most household uses [*Persson*, 1998, p. 97].

For a fault with asperities that are intermittently in contact during rupture, the average asperity height ΔH may be of the same order as the average gap height H. The expression for the lubrication pressure would reduce to

$$P_L \sim \frac{6\eta U L}{H^2}. \tag{14}$$

However, the assumption that the mean asperity height ΔH is of the same order as the initial gap height H_0 is not always valid for natural surfaces. As discussed above, $\Delta H = KL$ for a general class of self-similar rough surfaces. It follows from (13) that

$$P_L \sim \frac{6\eta U K L^2}{H^3}. \tag{15}$$

For natural fault surfaces and large ruptures (earthquake magnitude $M_w > 6$) the parameter K is of the same order as H/L. As will be discussed below, lubrication pressure is only significant for large earthquakes. Therefore (14) is often a convenient approximation for the lubrication pressure.

The effectiveness of lubrication is evaluated by normalizing (15) by the pressure from the static load to form the dimensionless Sommerfeld number,

$$S \equiv \frac{P_L}{P} = \frac{6\eta U L^2 K}{P H^3}, \tag{16}$$

where P is the lithostatic pressure for geological problems [*Sommerfeld*, 1950]. This form of the Sommerfeld number is slightly modified from the original reference because of the geometric difference between the axisymmetric journal bearing problem that Sommerfeld was considering and the natural, planar fault considered here.

The average gap height H is equal to the sum of the initial average gap height H_0 and the average elastic displacement D. According to Hooke's law, D is related to the lubrication pressure by

$$D = LP_L/E, \tag{17}$$

where E is Young's modulus. For small lubrication pressures the elastic displacement is negligible, and

$$S = \frac{6\eta U K L^2}{(H_0)^3}\frac{1}{P}. \tag{18}$$

The initial gap geometry drives the lubricating flow, and the asperities are undeformed. This regime occurs when the lubrication pressure is much less than the pressure necessary to generate displacement of order H_0,

$$P_L \ll EH_0/L. \tag{19}$$

We define a critical lubrication length L_c below which the elastic displacement D is insignificant. L_c is defined as the length at which $D = H_0$. Combining (15) and (17),

$$L_c = 2H_0\left(\frac{H_0 E}{6\eta U K}\right)^{1/3}. \tag{20}$$

In the inelastic regime where $L \ll L_c$, the larger the value of L, the larger the lubrication pressure.

For large $L \gg L_c$, elastic displacement is significant. The initial gap height H_0 is much less than D and the total gap height H is primarily determined by the elastic contribution, i.e., $H \approx D$. The roughness K is assumed constant, and therefore for $L \gg L_c$,

$$S = \left(\frac{6\eta U K E^3}{L}\right)^{1/4}\frac{1}{P}. \tag{21}$$

Equation (21) indicates that S decreases with increasing L in the elastic regime. As the value of L increases, the elastic displacement widens the gap, and therefore the lubrication pressure gradually decreases. This decrease of lubrication pressure in the elastic regime is a gradual process ($P_L \sim L^{-1/4}$) since the decreasing lubrication pressure also reduces the strain, D/L.

The Sommerfeld number measures the importance of lubrication in determining the frictional properties of a system. To show this, we compute the effective coefficient of friction $\mu \equiv \tau_f/P$ where τ_f is the frictional stress and P is the lithostatic pressure. We use the classical model of *Hubbert and Rubey* [1959] describing the effects of pore fluid pressure. The effective pressure P_e on the solid contacts is the static load less the average

pore pressure P_p [*Hubbert and Rubey*, 1959],

$$P_e = P - P_p. \tag{22}$$

The average frictional stress τ_f on contacting asperities is

$$\tau_f = \mu_s P_e, \tag{23}$$

where μ_s is the solid coefficient of friction, a material property of the solid surface. The *Hubbert and Rubey* [1959] model, like nearly all frictional models, is based on the observation that contacting asperities account for the majority of the frictional stress even though they comprise only a small fraction of the fault plane area. This work adds the effect that during rupture the pore pressure is dynamically increased and $P_p = P_p^0 + P_L$.

For small Sommerfeld numbers the lubrication pressure supports an insignificant fraction of the load. The two sides of the fault are in contact at asperities and conventional formulations of solid friction as proportional to the normal stress are appropriate. This limiting behavior is known as boundary layer friction. The frictional stress τ_f is determined by adhesive forces and can to some extent be predicted from the surface chemistry [*Persson*, 1998]. In the boundary layer friction regime, $P_e = P$ and $\mu = \mu_s$. To date, most frictional experiments for geophysical applications have been in this regime.

For large Sommerfeld numbers the lubrication pressure completely supports the load and no normal stress is exerted on contacting asperities. The only frictional stress is the viscous resistance of the fluid and (23) is not relevant. The magnitude of the viscous stress in the fluid is $\eta \partial u/\partial z$. Equation (2), which is the lubrication equation of motion in the x direction, shows that the velocity gradient $\partial u/\partial z$ scales as $P_L H/L\eta$. Therefore the viscous stress scales as $P_L H/L$. Since the viscous stress is the only frictional stress in the fully lubricated regime,

$$\mu = SH/L, \tag{24}$$

where the definition of the Sommerfeld number as $S = P_L/P$ has been used to simplify the expression.

Between the boundary layer and the hydrodynamic regimes is the "mixed regime." Friction is determined by a mixture of viscous resistance and solid asperity contacts (Figure 1). The effects are additive and the frictional stress is

$$\tau_f = \mu_s P_e + SPH/L. \tag{25}$$

If we neglect the initial hydrostatic fluid pressure P_p^0 for the purposes of this qualitative discussion of friction, then $P_e \approx P(1-S)$ and the effective frictional coefficient is

$$\mu = \mu_s(1 - S) + SH/L. \tag{26}$$

All three types of behavior are shown schematically in the classical Stribeck curve in Figure 7 [*Spikes*, 1997] and are summarized by

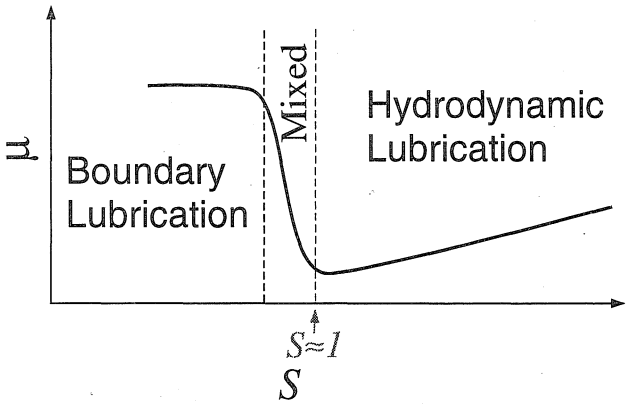

Figure 7. The Stribeck curve schematically shows the variation of the coefficient of friction μ with S. In the region labeled "boundary lubrication," solid-solid friction predominates. Between the dashed lines is the mixed regime where solid-solid friction is reduced by the lubrication pressure. In the "hydrodynamic lubrication" region, solid-solid friction is eliminated, and the friction is determined by the viscous stress.

$$\mu = \begin{cases} \mu_s & S \ll 1 \\ \mu_s(1 - S) + SH/L & S \approx 1 \\ SH/L & S \gg 1. \end{cases} \tag{27}$$

The Stribeck curve demonstrates both effects of lubrication outlined in section 1. In the hydrodynamic regime the shear stress is low since solid-solid friction has been eliminated in favor of viscous effects. In the mixed regime the friction has been depressed since the lubrication pressure is high.

6. Physical Constraints on Parameters

We now estimate the values of the parameters in (16), (17), and (20) in order to quantify the lubrication effect during earthquakes. The value of viscosity depends on the fault fluid. A number of studies have shown that crustal fluids migrate to highly permeable fault zones [*Davis and DeWiest*, 1966], and there is reason to believe that aqueous fluids are abundant at midcrustal levels due to metamorphic reactions [e.g., *Rumble*, 1994]. If the lubricant during an earthquake is H_2O, the viscosity is on the order of 10^{-3} Pa s [*Sengers and Watson*, 1986]. Alternatively, solid-solid frictional stresses may melt the wall rock during the early stages of an earthquake as first suggested by *Jeffreys* [1942]. Such a melt would be a viable lubricating fluid with a viscosity of at least 10 Pa s [*Spray*, 1993]. In this case, thermal effects should be considered in addition to the strictly mechanical lubrication addressed here. We favor a slurry formed from the mixture of fine-grained gouge with H_2O as the lubricant for the reasons noted in section 1. There is evidence of slurries in fault zones and they are probably viscous enough to produce significant lubrication. *Major and Pierson* [1992] showed that at shear strain rates >5 s^{-1} and atmospheric pres-

Table 1. Typical Parameter Ranges

Parameter	Values
η	10 Pa s
U	1 m/s
K	10^{-3}
L	$(M_0/M_0^0)^{1/3}$ m[a]
H_0	10^{-3} m
E	5×10^{10} Pa
P	1–2 $\times$ 10^8 Pa

[a] M_0^0 is the moment of a $M_w = 6$ earthquake (1.3×10^{18} N m) and is used to normalize the slip distance to be 1 m for such an event.

sure, fine-grained slurries exceed their yield strengths and behave as Newtonian fluids with constant effective viscosities. Since the shear strain rates during rupture are on the order of 1000 s^{-1}, we expect the fluid to be in this Newtonian regime even if some increase of yield strength occurs with confining pressure. The observation of eddy structures in fault zone cataclasites gives further evidence that gouge fluidizes during rupture [*Otsuki*, 1999]. Slurries with mean grain diameters <63 μm had viscosities of 0.2 to 7.1 Pa s at atmospheric pressure in the experiments of *Major and Pierson* [1992]. We expect the viscosity to increase somewhat at depth and therefore estimate the slurry viscosity to be 10 Pa s. *Major and Pierson* [1992] also showed that slurry viscosity is extremely sensitive to solid volume fraction and can change by an order of magnitude if the solid volume fraction changes from 45% to 50%. As a result our estimate of viscosity is necessarily approximate, and we acknowledge that it may be inaccurate by a factor of 10 or more.

An average value for slip velocity for moderate earthquakes is 1 m/s [*Lay and Wallace*, 1995]. This standard value is adopted for most of this study. A preliminary model incorporating variable velocity is also explored in this paper under the discussion of radiated energy data as a model application. This more complete treatment includes velocity variations consistent with the variations in friction due to lubrication.

The aspect ratio K is observed to be 10^{-4}–10^{-2} in the data of *Power and Tullis* [1991]. The profiles studied range from 10 μm to 40 m. In the absence of more precise data we select $K = 10^{-3}$ as a representative value. Note that the f^{-2} spectrum used here is not used by the authors of *Power and Tullis* [1991] in their analysis, but it is consistent with the data for each profile presented in their paper.

The lubrication length L is approximately equal to the slip distance d as discussed above. The slip distance d scales as $M_0^{1/3}$, where M_0 is the seismic moment [*Kanamori and Anderson*, 1975]. We assume that the slip for a $M_w = 6$ earthquake is 1 m. This approach uses the final slip distance as L and therefore calculates the maximum value of the Sommerfeld number S for a given magnitude earthquake.

The average initial gap height H_0 is assumed to be comparable to observed geological features that are inferred to have been generated during a single slip event. Such features include intravein septa, slickenslide surfaces, and occasionally pseudotachylytes. All of these features often indicate sliding localized to regions on the scale of millimeters [*Sibson*, 1999]. Therefore we take $H_0 = 1$ mm.

The elastic modulus E is a material parameter of the rock and is 5×10^{10} Pa for a typical granite [*Carmichael*, 1982]. Ambient pressure is estimated as the lithostatic value at the hypocenter. Typical values in the seismogenic zone are 1–2$\times 10^8$ Pa. More precise estimates can be made for specific events by using the hypocentral location.

The parameters listed above are summarized in Table 1 and result in values of the Sommerfeld number on the order of 0.1 for moderate earthquakes. These values indicate that the rupture process overlaps with the dynamic regime in which variations in lubrication pressure are significant. Values for a few representative events are listed in Table 2.

Combining the above constraints and using the standard relationship between seismic moment and magnitude,

$$\log M_0 = 1.5 M_w + 9.1, \tag{28}$$

Table 2. Sommerfeld Numbers for Representative Earthquakes[a]

Earthquake	Date	M_w	U, m/s	d, m	P,[b] 10^8 Pa	S	Reference[c]
Landers	June 28, 1992	7.2	1	7	1.9	0.1	1
Northridge	January 17, 1994	6.7	1	3.2	4.7	0.1	2
Parkfield	December 20, 1994	4.7	1.1	0.77	2.4	0.1	3

[a] In order to provide consistent comparisons, Sommerfeld number is computed for the maximum observed velocity and slip. Parameters omitted from this table are taken to be the typical values in Table 1.
[b] Values for P are based on hypocentral depths.
[c] References: (1) *Wald and Heaton* [1994], (2) *Wald et al.* [1996], and (3) *Fletcher and Spudich* [1998].

where M_0 has units of N m, we graph a relationship between Sommerfeld number and magnitude (Figure 8). Lubrication pressure can reach 30% of the lithostatic pressure for large earthquakes with typical fault parameters, but lubrication is negligible for small earthquakes.

Parameters in Table 1 are approximate, and Figure 8 shows the sensitivity of the results to errors in the estimates. The least constrained parameters, η and H_0, are varied. The results are very sensitive to the parameters chosen for small earthquakes and more robust for large earthquakes. Despite the variation, small earthquakes remain essentially unlubricated in all cases. The significant lubrication pressures in moderate to large events are relatively insensitive to variations in parameters because of the limiting effect of the elastic deformation. This result is consistent with the scaling argument in (21) where the Sommerfeld number is shown to be proportional to the 1/4 root of most parameters.

7. Model Applications

The paper to this point has presented a conceptual overview of hydrodynamic lubrication, a mathematical model, and the necessary quantification of parameters. We now use lubrication theory to explain the following three observations: low heat flow on the San Andreas, along-strike variations in strong motion spectra, and a difference in scaled radiated energy between large and small earthquakes. After discussing each application separately, we present an optimized parameter set that is consistent with all three applications.

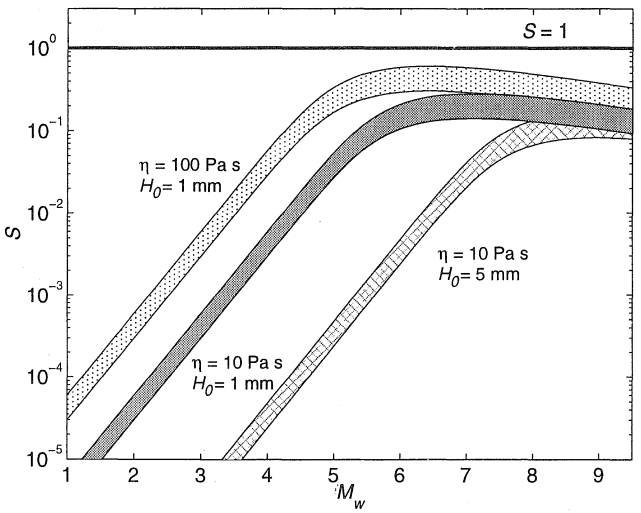

Figure 8. Dependence of Sommerfeld number on magnitude M_w. The solid area is calculated with the typical parameters in Table 1. The upper and lower bounds are determined by the range in lithostatic pressure P. The other two regions show the sensitivity of the results to varying parameters. Both are also calculated with the parameters of Table 1 except η=100 Pa s in the stippled area and H_0=5 mm in the cross-hatched area.

Table 3. Frictional Stress[a]

Case	P_p^0, 10^7 Pa	P_L, 10^7 Pa	τ_f, 10^7 Pa
a	0	0	10
b	7	0	7
c	7	3	5
d	7	10	0.9

[a]Minimum frictional stress on the fault τ_f computed from Byerlee's law (29) for different assumptions. The cases are case a, dry rock; case b, hydrostatic pore pressure only; case c, lubrication with typical parameters; and case d, lubrication with η=350 Pa s.

7.1. Heat Flow

Heat flow measurements across the San Andreas fault require that the frictional stress on the fault is less than 10^7 Pa at 7 km depth [*Lachenbruch and Sass*, 1980]. This strong constraint on the fault energetics is puzzling in light of laboratory data on rock friction. According to laboratory experiments the frictional stress τ_f between rock surfaces is determined by Byerlee's law

$$\tau_f = \mu_s P_e = \mu_s (P - P_p^0 - P_L), \qquad (29)$$

where the coefficient of friction μ_s is between 0.6 and 0.85 and the effective pressure is as defined in (22). At an average seismogenic depth of 7 km with hydrostatic fluid pressure ($P = 1.9 \times 10^8$ Pa, $P_p^0 = 7 \times 10^7$ Pa), Byerlee's law requires the frictional stress to be at least 7×10^7 Pa (Table 3). A dynamic increase in fluid pressure of 10^8 Pa, i.e., $S = 0.5$ is required in order to solve the friction paradox. The parameters considered in Table 1 allow a maximum lubrication pressure $P_L = 3 \times 10^7$ Pa. Dynamic lubrication in this situation reduces the friction by 30% relative to the hydrostatic value. This reduction is comparable to the reduction in friction from dry rock to the hydrostatic value and is therefore signficant. However, lubrication does not completely solve the friction paradox. Sufficient lubrication pressure can be achieved by lubrication using a higher viscosity slurry or melt with η = 350 Pa s. Alternatively, other mechanisms such as thermal pressurization in the confined fault zone might account for a portion of the dynamic fluid pressure increase [*Sibson*, 1973; *Lachenbruch*, 1980; *Mase and Smith*, 1987].

The calculations show that hydrodynamic lubrication is only significant for large earthquakes. A dynamic lubrication model for reducing frictional stress requires that the majority of slip on a fault occurs during the larger magnitude events. This is consistent with standard scaling relationships for seismic energy with magnitude [*Kanamori and Anderson*, 1975]. Moreover, the heat flow constraint is only applicable to large earthquakes [*Lachenbruch and Sass*, 1980].

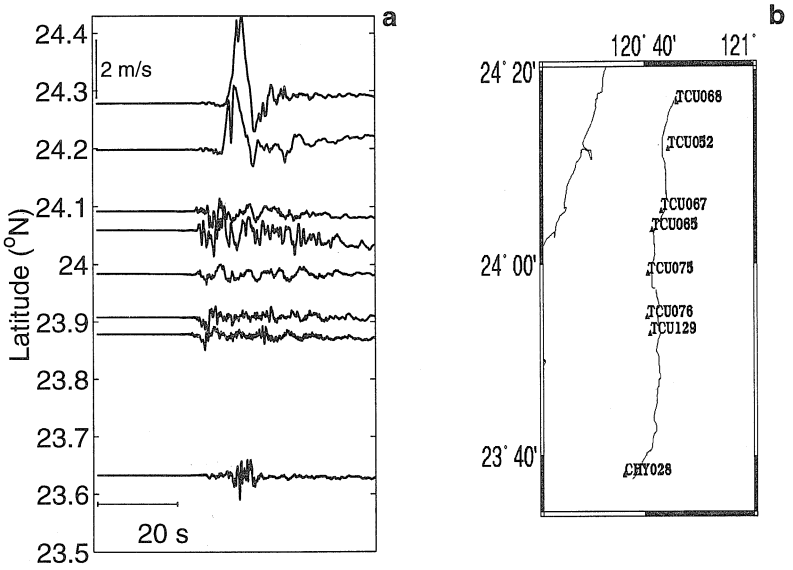

Figure 9. Velocity records from Chi-Chi, Taiwan $M_w = 7.6$ earthquake. (a) North component of velocity at stations within a few kilometers of the surface rupture. Velocity is integrated from acceleration records provided courtesy of Taiwan Meteorological Institute with a correction for instrumental drift late in the record. The y axis shows latitude of the stations. (b) Station map and surface rupture. Fault plane dips to the east.

7.2. Strong Motion Spectra

A unique set of strong motion records was recorded within a few kilometers of the surface rupture during the September 20, 1999, $M_w = 7.6$ Chi-Chi, Taiwan, earthquake (Figure 9). The earthquake is notable for its high particle velocities as well as the distinct lack of high-frequency energy in the areas with large velocities [*Ma et al.*, 1999]. The northern records are dominated by a smooth, large-amplitude pulse in velocity, whereas the southern ones have higher frequency energy with lower velocities. This difference in frequency content along-strike was also manifested as greater damage in the south, despite the larger displacements in the north. The damage patterns and mapped fault offsets confirm that the variation in the records is a result of along-strike trends rather than local site responses or amplified motion on the hanging wall.

We hypothesize that the high frequency energy is generated by contacting asperities (Figure 10). Collisions between asperities are accommodated by a combination of normal displacement and failure. Both processes radiate high frequency energy. Asperities that radiate energy by these processes must be much smaller than the slip distance. The rate of asperity contact controls the minimum frequency, f_c, of the displacement waves generated by asperity collisions. Therefore,

$$f_c \gg U/d. \tag{30}$$

Using the values in Table 4, we compute that for station TCU129, $f_c \gg 0.8$ Hz, and for TCU068, $f_c \gg 0.4$ Hz. On the basis of these values we define "high-frequency energy" as waves with frequencies >1 Hz.

The lubrication model can explain the observed data if the lubrication length scale L in the northern sec-

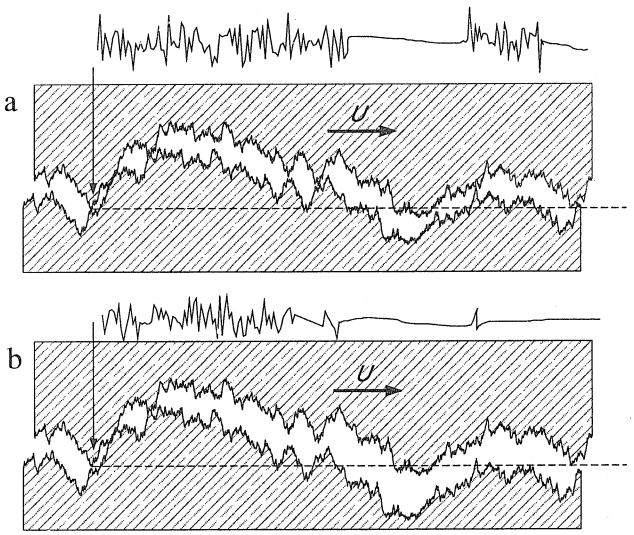

Figure 10. Vertically exaggerated cartoon illustrating asperities breaking during rupture. (a) Undeformed fault surface. As the point at the tip of the arrow slips to the right, it collides with the asperities on the lower surface above the dashed line. A schematic high-pass velocity trace for a station located at the arrow is shown at the top. (b) Deformed fault surface. There are fewer asperity contacts than in the undeformed case as shown by the shading and the velocity trace.

Table 4. Taiwan Station Parameters[a]

Station	d, m	U, m/s
TCU068	9.6	3.9
TCU052	8.7	2.7
TCU067	1.2	1.1
TCU065	1.6	1.5
TCU075	1.3	1.2
TCU076	1.3	0.87
TCU129	1.0	0.78
CHY028	1.3	0.94

[a]Observed maximum horizontal slip and particle velocity. Stations are arranged north to south as in Figure 9. The first two stations show anomalous "pulse" behavior.

tion of the fault was larger than the critical value L_c and therefore elastic displacement was significant. For a self-similar rough fault L is identical to the slip distance d as shown in Figure 5. It is hypothesized that at the northern stations $d \gg L_c$; therefore, the elastic deformation widened the fault and reduced asperity contact. High frequency radiation was reduced. Elsewhere on the fault d is hypothesized to have been less than L_c throughout the earthquake.

We verify the consistency of the hypothesis with the data by comparing the observed maximum slips (L) with the theoretical values of L_c from (20). Figure 11 shows the results calculated with the standard lubrication parameters in Table 1 combined with the velocities and slip distances in Table 4. The critical slip is between 1 and 2 m at all of the stations. L is shown to exceed L_c only at the two northernmost stations, and therefore the results are consistent with the lubrication hyopthesis. The values of L_c presented here depend on the estimates of the parameters in Table 1. However, (20) shows that the results are relatively insensitive to errors in all the parameters except H_0. The critical slip L_c is likely to be of the order of a few meters. Spectral analysis of the northern stations shows a falloff in frequency above ~1 Hz as would be expected from the lubrication model (Figure 12).

We predict that any large earthquake with slip distances greater than a few meters will have a zone of the fault that is well lubricated with depleted high-frequency energy. This behavior has direct implications for efforts to mitigate the effects of strong ground motion. Structures designed to withstand large earthquakes must accommodate large amplitude long-period motion but do not need to accommodate as much high-frequency energy as would be predicted from scaling the spectrum of small events. Of course, such theoretical predictions are preliminary and should be thoroughly validated before being incorporated into any design plans.

7.3. Radiated Energy

It has been observed in California that the ratio of radiated energy E_R to seismic moment M_0 is a function of magnitude (Figure 13) [*Abercrombie*, 1995; *Kanamori and Heaton*, 2000; *Prejean and Ellsworth*, 2001]. Large events ($M_w > 6$) have values of $E_R/M_0 \approx 10^{-4}$ while the small ones ($M_w < 4$) have values as low as 10^{-6}. This type of observation is extremely difficult, and the error increases for small events because of the model-dependent corrections for attenuation. Such corrections are necessary for accurate measurement of radiated en-

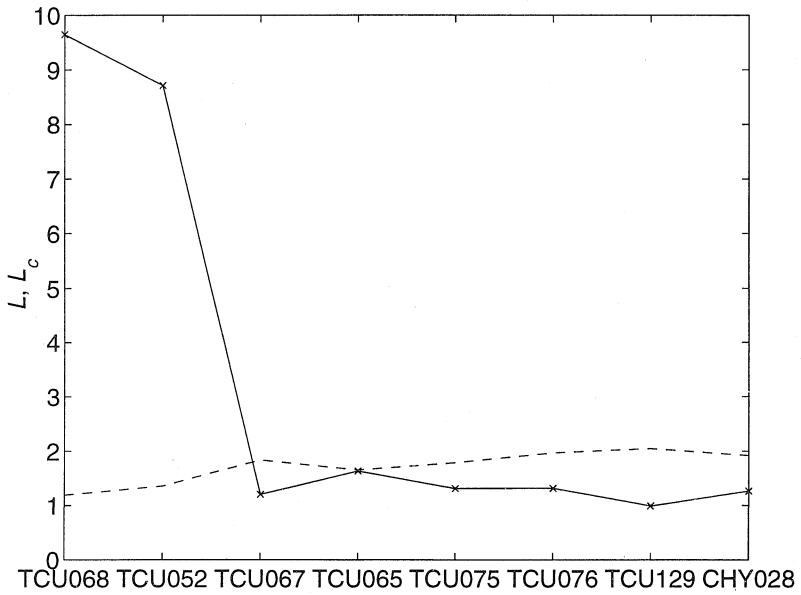

Figure 11. Comparison of observed maximum horizontal slip ($L = d$) at each station as tabulated in Table 4 (solid line) with the values of L_c computed using (20) (dashed line).

ergy and likely obscure the systematics for small earthquakes. We therefore only attempt to interpret the overall trend. There is a constant, large value of E_R/M_0 for large events, and a transition occurs at $M_w \approx 5$ to smaller values of the ratio for small earthquakes. We attempt to fit only the observed change of E_R/M_0 by a factor of 100 from M_w=4 to M_w=6.

The observations of scaled radiated energy have particularly important implications for slip velocity and therefore frictional behavior. Both *Sato and Hirasawa* [1973] and *Mott* [1948] derived a relationship between rupture velocity V_r, driving stress $\Delta\sigma_d$, and the observable ratio E_R/M_0, by calculating the kinetic energy during slip:

$$\frac{E_R}{M_0} = \frac{\Delta\sigma_d}{2G}\left(\frac{V_r}{\beta}\right)^2, \tag{31}$$

where G is the shear modulus and β is the shear velocity in the country rock outside the fault zone. The average driving stress during an earthquake is related to the initial stress σ_0 and the frictional stress σ_f by

$$\Delta\sigma_d = \sigma_0 - \sigma_f \tag{32}$$

and the frictional stress is reduced by the lubrication pressure. Therefore the driving stress is

$$\Delta\sigma_d = \sigma_0 - \mu_s P + \mu_s P_L. \tag{33}$$

The lubrication pressure P_L depends on the slip velocity U as shown in (15). The relative slip velocity is related to the driving stress in a propagating shear crack by

$$U = \Delta\sigma_d \beta/G \frac{2V_r/\beta}{E\left[\sqrt{1-(V_r/\beta)^2}\right]}, \tag{34}$$

where $E[]$ is the complete elliptic integral of the second kind [*Husseini*, 1977]. The derivation of (34) assumes that the driving stress is equal to the static stress drop. Here we assume that the equation is equally applicable for the instantaneous driving stress σ_d. A similar relationship is derived by *Kanamori* [1994] on the basis of kinematics. The details of (31) and (34) are model-dependent, but the basic functional relationships among σ_d, U, and E_R/M_0 are robustly determined by the kinematics of slip.

Combining (33), (34), and the definition of P_L in (15), we solve for U. The model nonlinearly couples the driving stress, slip velocity, and lubrication pressure. In Figure 14, solutions of S and U as a function of M_w are computed and then E_R/M_0 is derived using (31). The behavior of this model is best understood in terms of the critical slip distance L_c defined by (20). For the inelastic regime where $L < L_c$, as the slip distance increases, the lubrication pressure rises. For small magnitudes ($M_w < 4$) the lubrication pressure is much less than lithostatic pressure ($S \ll 1$), and there is little effect on the total frictional stress. Therefore velocity and E_R/M_0 are nearly constant in this magnitude range. For earthquakes with M_w>4 the lubrication pressure becomes a significant fraction of the lithostatic pressure and the frictional stress is reduced. Since the frictional resistance is less than in the unlubricated case, the driving stress is increased. The driving stress is coupled to U and E_R/M_0 in (31) and (34). Therefore U and E_R/M_0 also increase relative to their values for small events ($M_w < 4$).

For large-magnitude earthquakes ($M_w > 6$) where $L > L_c$ and elastic displacement is significant, the lubrication pressure decreases with increasing magni-

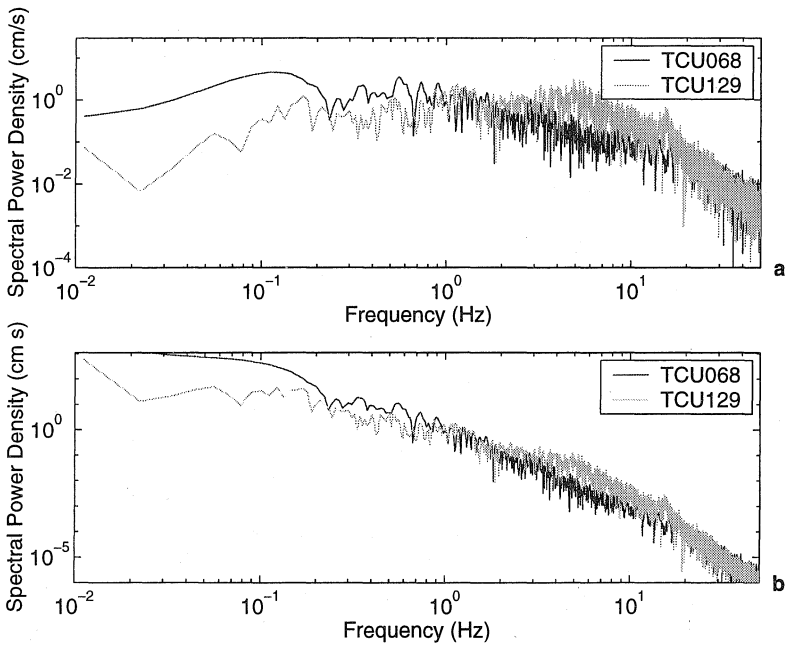

Figure 12. (a) Acceleration spectra for the Chi-Chi earthquake of the north component from a northern (TCU068) and southern (TCU129) near-fault station. (b) Displacement spectra derived from the acceleration records.

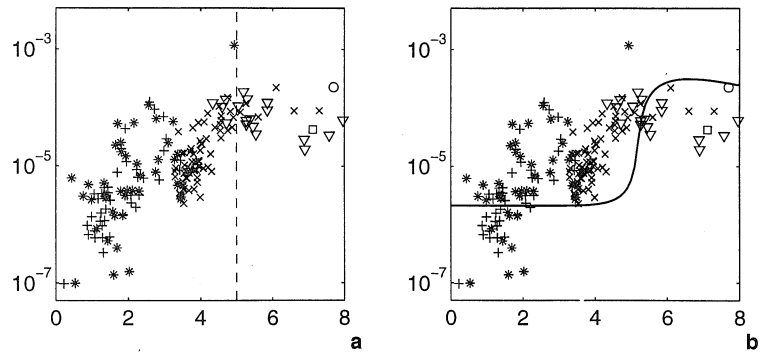

Figure 13. Observations of the ratio of locally measured radiated energy E_R to M_0. Data are from the following sources: stars, *Prejean and Ellsworth* [2001]; pluses, *Abercrombie* [1995]; crosses, *Kanamori and Heaton* [2000]; triangles, *Singh and Ordaz* [1994]; square, *Venkataraman et al.* [2000]; circle, *K.-F. Ma et al.*, manuscript in preparation. (a) Data separated into two regimes. To the right of the dashed line, E_R/M_0 is approximately constant and to the left it gradually decreases. Scatter also increases for the small events as discussed in the text. (b) Data and a solid line indicating the modeled values of E_R/M_0 using (16) and (31)–(34). We only attempt to fit the change in E_R/M_0 by a factor of 100 for M_w=4 to M_w=6. Parameters are as in Table 1 and as follows: $G = 2.0 \times 10^{10}$ Pa, $\mu_s = 0.6$, $P = 10^8$ Pa, $\sigma_0 = \mu_s P + 2 \times 10^5$ Pa, $V_r/\beta = 0.65$, $\beta = 3300$ m/s.

tude. The lubrication pressure P_L gradually decreases as $L^{-1/4}$ for large events in accordance with (21). The decrease in lubrication pressure results in a small increase in frictional resistance and therefore a decrease in the available driving stress. As a result, the slopes of the velocity and radiated energy curves in Figure 14 are slightly negative. At large magnitudes the model predicts a gradual decrease in radiated energy with increasing magnitude. This decrease is not observed, but the trend is much smaller than the scatter in the data.

We noted above that the increase in scatter for small earthquakes may be due to the methods used to measure radiated energy for small events. We speculate that there may also be real variability in E_R/M_0 for small events due to variations in parameters in the unlubricated regime. In the lubricated regime the system is insensitive to differences in the fault properties as shown in Figure 8 and (21). The scatter in E_R/M_0 data for large earthquakes is therefore small.

The earlier calculation of Sommerfeld number versus magnitude in Figure 8 appears to be superseded by Figure 14. However, Figure 14 contains more model-dependent assumptions embedded in (31)–(34). We have therefore chosen to present both forms of the relationship between M_w and Sommerfeld number S.

7.4. Optimized Parameters

Table 5 contains an optimized set of values for the 11 parameters in the model that satisfies all three observations discussed in this paper. The results for each ap-

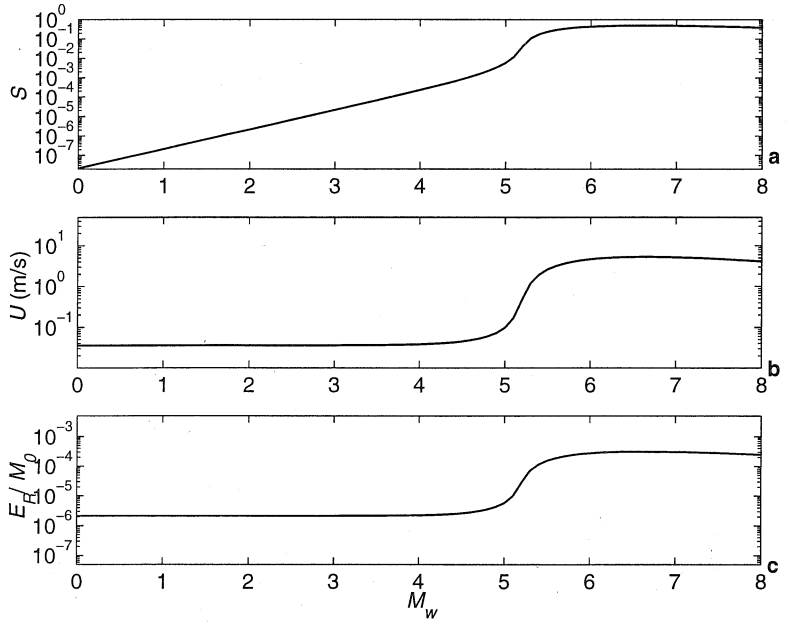

Figure 14. Dynamic friction model results. Frictionally controlled (a) Sommerfeld number, (b) slip velocity and (c) radiated energy as a function of magnitude. Parameters are as in Figure 13.

Table 5. Optimized Parameters

Parameter	Values
η	50 Pa s
U	see (34)
K	2×10^{-3}
L	$(M_0/M_0^0)^{1/3}$ m
H_0	2×10^{-3} m
E	5×10^{10} Pa
P	1×10^{8} Pa
G	2.0×10^{10} Pa
μ_s	0.6
σ_0	6.01×10^{7} Pa
V_r/β	0.8
β	3.3 km/s

plication are summarized in Figure 15. The approach taken in this section is to find parameters that match all of the datasets reasonably well instead of assigning the typical values of Table 1 a priori. No formal optimization algorithm was used since the fit is nonunique. The values in Table 5 are merely one representative set that can match all three data sets. The major difference between the optimized and typical parameter sets is that the viscosity is larger in the optimized set by a factor of 5. Since small changes of the particle concentration can change the slurry viscosity by an order of magnitude, we consider this adaptation reasonable.

In this combined model, the slip velocity is coupled to the frictional stress using (33)–(34). The dynamic model results in higher values of S for large events than were calculated in Figure 8 or Table 3. For the coupled model η=50 Pa s rather than η=350 Pa s is sufficient to explain the heat flow paradox.

All three model applications demonstrate the most important prediction of elastohydrodynamic lubrication theory. Large earthquakes behave qualitatively differently than small ones. Events with slip distances greater than ~0.5 m have low dynamic friction, fewer asperity-asperity contacts, and a larger proportion of the energy radiated.

8. Discussion

Now that the magnitude of the hydrodynamic lubrication effect is calculated, it is appropriate to review the assumptions about the fluid dynamics that were incorporated into the model. It is assumed that the fluid forms a continuous layer of constant initial height in the gap between moving, subparallel surfaces. This fluid may be a slurry which forms during the initiation of the earthquake. The duration of the earthquake is assumed to be much longer than the time necessary for fluidization. In the lubricating layer a continuum approximation is assumed to be appropriate. The sediment particles in the slurry are much smaller than the gap height. In the far-field where there is no slip, the pressure remains at the preearthquake level. The transition from the slipping to nonslipping zone is not explicitly modeled and is assumed to have only local effects. Additional complications could be added to the model and are likely to perturb the results presented here. The purpose of this study is to present a new concept in fault mechanics along with the minimum necessary quantification. Further refinements are clearly possible, but here we confine ourselves to only a brief evaluation of a few of the possible complicating factors.

The most significant adaptation of the standard engineering theory presented in this paper is the formulation for a self-similar rough fault. Alternative derivations are possible. For instance, when the elastic deformation of the wall is significant, the average asperity height ΔH may scale as the elastic displacement D instead of the original asperity height KL. In this case (17) must be substituted into (13) to derive an alternative form for the Sommerfeld number. This alternative formulation gives nearly identical results for the parameters used here. The limiting effect of the elastic deformation still determines the maximum lubrication pressure for large events. For both formulations this lubrication pressure is reached when the slip distance is much greater than ~0.5 m.

In the lubricated fault, fluid flows into a narrow gap, and the pore pressure dynamically increases. The permeability of the surrounding rock is sufficiently low that the fluid is effectively confined by the walls. This model

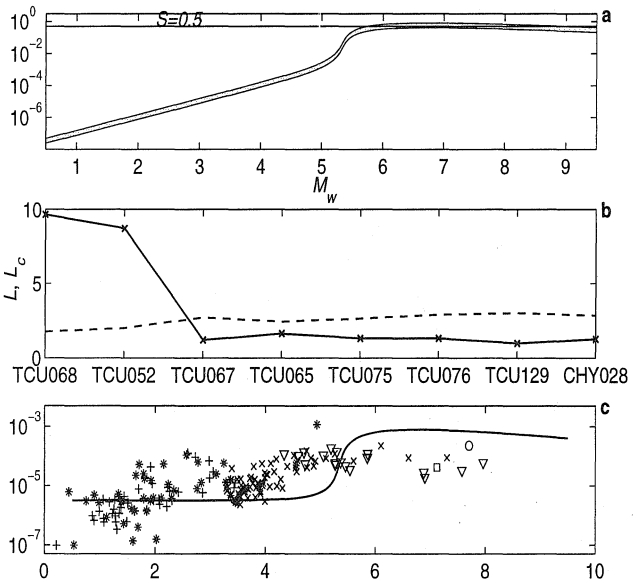

Figure 15. All three model applications with an optimally selected parameters set from Table 5. (a) Sommerfeld number as a function of M_w used to match heat flow data. S is calculated using (33)–(34). (b) Observed lubrication length at each station compared to the theoretical critical value computed using the optimized parameters and the observed maximum velocities in (20). (c) Predicted E_R/M_0 as a function of M_w and observed values. The calculated E_R/M_0 changes by a factor of 300 from M_w=4 to M_w=6.

is clearly an idealized end-member. In the natural system some leakage occurs during faulting to reduce the lubrication pressure. Such reductions can be included numerically as they are in the porous bearing of *Kaneko et al.* [1999] or the thermal pressurization calculations of *Lachenbruch* [1980]. Note that the fluid pressures calculated for the typical parameters of Table 1 are at most 40% lithostatic and therefore insufficient to produce hydrofractures as a means of releasing pressure. The optimized parameter set produces higher pressures and may result in hydrofracture.

Common lubricants in engineering applications have pressure-dependent viscosities where the viscosity increases with pressure. This has the effect of increasing the lubrication pressure as there is a positive feedback in the process. Similar behavior might be expected for fault slurry, but silicate melt viscosity decreases with pressure [*Kushiro*, 1980]. Therefore any identification of the fault fluid as melt must carefully consider whether the pressure-dependent viscosity would eliminate the lubrication effect.

The two-dimensional fault model neglects flow perpendicular to the slip direction. Such "side leakage" for a lubricated gap with equal length and width can reduce the fluid gap height by a factor of 2–3 for a constant load [*Hamrock*, 1994, p. 483]. It is not clear what the effect would be in the case of a fault where the fluid layer height is constant and the load varies. The rough faults that are modeled here are much wider than they are long ($a \gg L$) and side leakage should be reduced.

Contacting asperities set much more complex boundary conditions than are addressed here. A fully coupled solid-fluid model is required for a rigorous and complete study. The theoretical and numerical underpinnings of such models are at the forefront of current research in tribology [*Spikes*, 1997; *Jiang et al.*, 1999]. A full model might also be able to address the correct scaling in a rough fault that is not well matched at the initiation of the earthquake. A self-similar fault that is not well matched cannot be analyzed by the scaling arguments used here. A full model with an accurate representation of a specific fault's geometry is needed.

The normal velocity of the wall, V, is neglected in the form of the Reynolds equation used here. This approximation is valid if $V \ll UH/L$ [*Leal*, 1992]. The quasi-static model used for the elastic deformation also assumes that V is small; therefore the model is self-consistent. A fully dynamic calculation may show that the wall velocity is important in modifying the lubrication pressure.

In bearings, the lubricating fluid is seldom able to support negative dynamic pressures [*Dowson and Higginson*, 1977]. A combination of cavitation and exsolution of dissolved gases maintains the pressure at the initial reservoir level in strongly diverging channels. Cavitation is not expected to occur on a fault with a large confining pressure, but exsolution may be possible. If exsolution occurs and prevents negative dynamic pressures, then the net effect of hydrodynamic lubrication is much greater than calculated here.

Another possible complication is the compressibility of the fluid. Since the lubrication pressure is at most of the order of the initial hydrostatic pressure, the effects of compressibility on the pressure distribution are expected to be small [*Szeri*, 1998]. *Dowson and Higginson* [1977] showed for rectangular elastohydrodynamic conjunctions that fluid compressibility has no significant effect on the elastic deformation, although the pressure distribution is slightly different than in the incompressible case. Preliminary numerical experiments suggest that these results are also applicable to the rough fault studied here, but more work would be necessary to fully exclude the importance of compressibility.

As the fluid is squeezed through the narrow gap, dissipative heating occurs that may increase the temperature of the system. At the same time, the thermal expansion would increase the fluid pressure if there is abundant aqueous fluid. This thermal pressurization only occurs in the presence of ample aqueous fluid, whereas mechanical lubrication can occur with predominantly gouge. We calculate that the temperature rise due to frictional heating with thermal pressurization is $<60°$C by using the simplified equations of *Lachenbruch* [1980] without percolation or pore dilatation. This moderate thermal effect could decrease lubrication by decreasing the viscosity.

Additional complications could arise if the fluid is non-Newtonian and the viscosity depended upon the shear rate [*Jacobson*, 1991]. Inelastic effects such as wear of the wall rock and the generation of gouge may also be important.

9. Conclusions

We have shown in this paper that the mechanical effect of a viscous fluid lubricating a fault zone has implications for the rupture dynamics. Lubrication with typical parameters reduces the frictional stress during an earthquake by as much as 30% relative to the hydrostatic value or 50% relative to the dry rock friction. The heat flow paradox is completely solved if either the fault fluid has a viscosity of 350 Pa s or the friction is coupled to the dynamics with a fluid viscosity of only 50 Pa s. Dynamic widening of the fault reduces the radiation of high-frequency (>1 Hz) energy for earthquakes with large slips. The 2 orders of magnitude difference in the ratio of radiated energy to moment between small and large earthquakes is interpreted to reflect the lubrication-controlled frictional properties. All of these applications utilize the variation in lubrication behavior between small and large slip events. This change in behavior at the critical slip distance L_c is one of the most intriguing consequences of this theory and warrants further study.

The hydrodynamic lubrication mechanism outlined here indicates that the static values of pore pressure are

not appropriate for studies of earthquake rupture. The lubrication effect is present in all fluid-filled faults and is independent of any assumptions about the thermal effects of fault friction. Pore pressure must be viewed as a dynamic quantity, and prerupture values should not be used for modeling coseismic friction.

Appendix A: Elastic Solution

Since $H/L \ll 1$ we make the standard assumption that the displacement on the rough surfaces from a pressure source is approximately the displacement of a halfspace subject to vertical loading [e.g., *Hamrock*, 1994; *Dowson and Higginson*, 1977]. The solution for the displacement from a force of magnitude F applied at the origin normal to the free surface of an elastic halfspace [*Timoshenko and Goodier*, 1970],

$$w(r) = \frac{F(1-\nu^2)}{\pi E r}, \tag{A1}$$

where $w(r)$ is the vertical displacement on the free surface at a distance r from the origin and E is Young's modulus. This is equivalent to a pressure source $p(x, y)$ applied at a point,

$$p(x,y)\delta_d(x)\delta_d(y) = F \tag{A2}$$

where $\delta_d()$ denotes a Dirac delta function.

The displacement from a finite line on the y axis with ends at $y = \pm a$ is the sum of the point source terms (Figure A1). If the pressure is constant in the y direction, i.e., $\partial p/\partial y = 0$, the displacement at a point on the x axis that is a distance r from the origin is

$$w(r) = 2\int_{y=0}^{a} \frac{(1-\nu^2)p(x)}{\pi E r} dy\ . \tag{A3}$$

If the finite line source is at $x = \xi$, the displacement $w(x)$ in a Cartesian coordinate system is

$$w(x) = 2\delta_d(\xi)\int_{y=0}^{a} \frac{p(\xi)(1-\nu^2)}{\pi E\sqrt{(x-\xi)^2+y^2}} dy. \tag{A4}$$

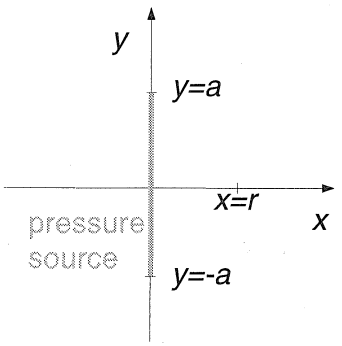

Figure A1. Geometry for calculating displacement from an finite line source of pressure. In the geological case, the x-y plane is the fault plane. Slip is in the x direction.

After performing the integration the displacement is explicitly

$$w(x) = \frac{2p(\xi)(1-\nu^2)}{\pi E}\delta_d(\xi)\ln\left|\frac{a+\sqrt{(x-\xi)^2+a^2}}{x-\xi}\right|. \tag{A5}$$

The displacement from a pressurized fault of length L is the integration of (A5) over every point $x = \xi$. The change in total gap height $\delta(x)$ combines contributions from both walls,

$$\delta(x) = \frac{4(1-\nu^2)}{\pi E}\int_0^L p(\xi)\ln\left|\frac{a+\sqrt{(x-\xi)^2+a^2}}{x-\xi}\right| d\xi. \tag{A6}$$

In the model described in the text, for single asperities we assume that the lubricated zone is equidimensional and therefore $2a = L$. For rough surfaces we use a constant width $a = \mathcal{L}/2$. Since $\mathcal{L} \gg d$ in the calculations, the lubricated zone for rough surfaces is much wider than the length in the x direction. Slip zones that are longer in the slip normal direction than the slip direction are suggested by the seismological observation of *Heaton* [1990]. They are also consistent with the two-dimensional Reynolds equation in (6).

Appendix B: Numerical Method

Incorporating elastic deformation into lubrication in a thin gap requires the simultaneous solution of the Reynolds equation (6) and the elastic displacement of the boundaries (8). The gap height $h(x)$ is related to the initial gap height $s(x)$ and the elastic displacement $\delta(x)$ by

$$h(x) = s(x) + \delta(x). \tag{B1}$$

These equations are to be solved with the boundary conditions

$$\begin{aligned} p(x=0) &= 0 \\ p(x=L) &= 0. \end{aligned} \tag{B2}$$

B1. Reynolds Equation

In the absence of elastic deformation, the Reynolds equation is solved in its integrated form

$$p(x) = 6\eta U\int_0^x \frac{h^* - h}{h^3} dx + p_p^0. \tag{B3}$$

We use the boundary conditions (B2) to solve for the integration constant h^* in (B3). As discussed before, the pressures are referenced to the level where $p_p^0 = 0$. The boundary condition at $x = L$ is $p = 0$, which implies that

$$h^* = \frac{\int_0^L \frac{1}{h^2} dx}{\int_0^L \frac{1}{h^3} dx}. \tag{B4}$$

In order to numerically solve for p we use a discretization of (B3) utilizing the trapezoidal rule [*Abramowitz*

and Stegun, 1965]

$$\tilde{p}_i = -6\eta U \sum_{j=1}^{i-1} \left(\frac{h_j - h^*}{h_j^3} + \frac{h_{j+1} - h^*}{h_{j+1}^3} \right) \frac{\Delta x}{2} \quad \text{(B5)}$$

where $\Delta x \equiv x_{i+1} - x_i$ and $\tilde{p}_i$ is the solution to the Reynolds equation for the pressure at $x = i\Delta x$. In the absence of elastic deformation, $h(x) = s(x)$, where $s(x)$ is the initial gap height function.

B2. Elastic Displacement

The elastic equation (8) is discretized as

$$\delta_i = \frac{4(1-\nu^2)\Delta x}{\pi E} \cdot \sum_{j=1}^{N} p_j \ln \left| \frac{L/2 + \sqrt{(L/2)^2 + (x_{i+1/2} - x_j)(x_{i-1/2} - x_j)}}{\sqrt{(x_{i+1/2} - x_j)(x_{i-1/2} - x_j)}} \right| \quad \text{(B6)}$$

where N is the number of grid points. The terms $x_{i+1/2}$ and $x_{i-1/2}$ are introduced following *Okamura* [1983] to handle the singularity where $x_i = x_j$.

Elastic displacement is combined with the Reynolds equation using an iteration scheme with damping. Instead of using the full computed $\tilde{p}(x)$ from (B5), a portion of the calculated pressure is added at each step. The pressure distribution for step $k + 1$ is calculated based on the pressure at step k by

$$p_i^{k+1} = p_i^k + \omega(\tilde{p}_i - p_i^k), \quad \text{(B7)}$$

where ω is a damping factor between 0 and 1. For gaps with an initial average height of 0.1 mm, ω must be 0.01 or less during the first two steps for convergence to be achieved in the majority of cases. After the initial few steps, the problem becomes more stable and the degree of damping can be reduced adaptively. For randomly generated rough surfaces, ω=0.01 is occasionally insufficient and the calculation does not converge. The hydrodynamic code and iteration scheme were verified with analytic and approximate solutions for a planar slider like that shown in Figure 3.

The full scheme for computing iteration step k is as follows:

1. An initial gap height $s(x)$ is chosen and calculated as a function of x.

2. The deformed gap height $h(x) = s(x) + \delta(x)$ is calculated. During the first iteration $\delta(x)$ is assumed to be 0 everywhere, so $h(x) = s(x)$.

3. The integrated, discretized Reynolds equation in (B5) is solved for $\tilde{p}(x)$ using the geometry given by $h(x)$.

4. The new pressure $p^{k+1}(x)$ is calculated using (B7). Initially, $p(x) = \mathbf{0}$; therefore $p^{k+1}(x) = \omega\tilde{p}(x)$ in the first iteration.

5. The displacement $\delta(x)$ is calculated with (B6) using the new pressure distribution $p^{k+1}(x)$.

6. The convergence parameter Dif $\equiv (\tilde{p}_l - p_l^k)/p_l^{k+1}$ is evaluated at a point l. In the computations, we arbitrarily choose l such that $l = N/4$.

7. The damping factor ω is adapted based on the value of Dif. If Dif < 100, the value is increased by a factor of 10 and is further increased for each order of magnitude that Dif drops until a prescribed maximum value $\omega_{\max}$ is reached. In these computations $\omega_{\max} = 0.1$.

8. If Dif $> \epsilon$, where ϵ is a small number, return to step 2. The code used here has $\epsilon = 10^{-5}$.

Acknowledgments. We are indebted to Brad Sturtevant for numerous stimulating conversations and insightful comments that provided the foundation for this work. We dedicate this paper to his memory. Y. Ben-Zion, J. Brune, N. Sleep, and V. Lyakhovsky provided constructive reviews. This work was supported in part by the National Science Foundation grant NSF EAR-9909371 and the US Geological Survey grant USGS HQGR0035. The Taiwan data are taken from W.H.K. Lee, T.C. Shin, K.W.Kuo, and K.C.Chen, CWB Free-Field Strong-Motion Data from 921 Chi-Chi Earthquake: Volume 1, Digital Acceleration Files on CD-ROM. This is contribution 8700 of the Caltech Division of Geological and Planetary Sciences.

References

Abercrombie, R., Earthquake source scaling relationships for -1 to 5 M_L using seismograms recorded at 2.5 km depth, *J. Geophys. Res.*, *100*, 24,015–24,036, 1995.

Abramowitz, M., and I. Stegun, *Handbook of Mathematical Functions, with Formulas, Graphs, and Mathematical Tables*, Dover, Mineolas, N.Y., 1965.

Ben-Zion, Y., and D. Andrews, Properties and implications of dynamic rupture along a material interface, *Bull. Seismol. Soc. Am.*, *88*, 1085–1094, 1998.

Brown, S. R., and C. H. Scholz, Broad bandwidth study of the topographys of natural rock surfaces, *J. Geophys. Res.*, *90*, 12,575–12,582, 1985.

Brune, J., S. Brown, and P. Johnson, Rupture mechanism and interface sparation in foam rubbre models of earthquakes: A possible solution to the heat flow paradox and the paradox of large overthrusts, *Tectonophysics*, *218*, 59–67, 1993.

Byerlee, J., Friction, overpressure and fault normal compression, *Geophys. Res. Lett.*, *17*, 2109–2112, 1990.

Byerlee, J. D., Static and kinetic friction of granite at high normal stress, *Inst. J. Rock Mech. Min. Soc.*, *7*, 3821–3827, 1970.

Carmichael, R. S., ed., *Handbook of Physical Properties of Rocks*, vol. 2, CRC Press, Boca Raton, Fla., 1982.

Davis, S. N., and R. J. DeWiest, *Hydrogeology*, John Wiley, New York, 1966.

Dowson, D., and G. Higginson, *Elasto-Hydrodynamic Lubrication*, Pergamon, New York, 1977.

Fletcher, J., and P. Spudich, Rupture characterisitics of the three M ~ 4.7 (1992–1994) Parkfield earthquakes, *J. Geophys. Res.*, *103*, 835–854, 1998.

Hamrock, B. J., *Fundamentals of Fluid Film Lubrication*, McGraw-Hill, New York, 1994.

Heaton, T. H., Evidence for and implications of self-healing pulses of slip in earthquake rupture, *Phys. Earth Planet. Inter.*, *64*, 1–20, 1990.

Hubbert, M. K., and W. W. Rubey, Role of fluid pressure in mechanics of overthrust faulting, *Geol. Soc. Amr. Bull.*, *70*, 115–166, 1959.

Husseini, M. I., Energy balance for motion along a fault, *Geophys. J. R. Astron. Soc.*, *49*, 699–714, 1977.

Jacobson, B., *Rheology and Elastohydrodynamics Lubrication*, Elsevier Sci., New York, 1991.

Jeffreys, H., On the mechanics of faulting, *Geol. Mag.*, *79*, 291, 1942.

Jiang, X., D. Hua, H. Cheng, X. Ai, and S. C. Lee, A mixed elastohydrodynamic lubrication model with asperity contact, *J. Tribol.*, *121*, 481–491, 1999.

Kanamori, H., Mechanics of earthquakes, *Annu. Rev. Earth Planet. Sci.*, *22*, 207–237, 1994.

Kanamori, H., and D. L. Anderson, Theoretical basis of some empirical relations in seismology, *Bull. Seismol. Soc. Am.*, *65*, 1073–1095, 1975.

Kanamori, H., and T. Heaton, Microscopic and macroscopic physics of earthquakes, in *GeoComplexity and the Physics of Earthquakes, Geophys. Monogr. Ser.,* vol. 120, edited by J. Rundle, D. Turcotte, and W. Klein, pp. 147–183, AGU, Washington, D. C., 2000.

Kaneko, S., H. Takabatake, and K. Ito, Numerical analysis of static characteristics at start of operation in porous journal bearings with sealed ends, *J. Tribol.*, *121*, 62–68, 1999.

Kushiro, I., Viscosity, density, and structure of silicate melts at high pressures, and their petrological applications, in *Physics of Magmatic Processes*, pp. 93–117, Princeton Univ. Press, Princeton, N.J., 1980.

Lachenbruch, A. H., Frictional heating, fluid pressure and the resistance to fault motion, *J. Geophys. Res.*, *85*, 6097–6112, 1980.

Lachenbruch, A. H., and J. H. Sass, Heat flow and energetics of the San Andreas fault zone, *J. Geophys. Res.*, *85*, 6185–6222, 1980.

Lay, T., and T. Wallace, *Modern Global Seismology*, Academic, San Diego, Calif., 1995.

Leal, L., *Laminar Flow and Convective Transport Processes*, Butterworth-Heinemann, Woburn, Mass., 1992.

Ma, K.-F., C.-T. Lee, and Y.-B. Tsai, The Chi-Chi, Taiwan earthquake: Large surface displacements on an inland thrust fault, *Eos Trans. AGU*, *80*, 605–611, 1999.

Major, J. J., and T. C. Pierson, Debris flow rheology: Experimental analysis of fine-grained slurries, *Water Resour. Res.*, *28*, 841–857, 1992.

Mase, C. W., and L. Smith, Effects of frictional heating on the thermal, hydrologic, and mechanical response of a fault, *J. Geophys. Res.*, *92*, 6249–6272, 1987.

Melosh, J., Acoustic fluidization: a new geologic process?, *J. Geophys. Res.*, *84*, 7512–7520, 1979.

Mott, N. F., Fracture of metals: Some theoretical considerations, *Engineering*, *165*, 16–18, 1948.

Okamura, H., A contribution to the numerial analysis of isothermal elastohydrodynamic lubrication, in *Tribology of Reciprocating Engines: Proceedings of the 9th Leeds-Lyon Symposium on Tribology held in Bodington Hall, the University of Leeds, England, 7-10 September 1982*, edited by D. Dowson, pp. 313–320, Butterworths, London, 1983.

Otsuki, K., Thermal pressurization, fluidization and melting of fault gouge recorded in the rock from Nojima seismic fault, *Eos Trans. AGU*, *80*(46), Fall Meet. Suppl., F727, 1999.

Persson, B. N. J., *Sliding Friction: Physical Principles and Applications*, Springer-Verlag, New York, 1998.

Power, W. L., and T. E. Tullis, Euclidean and fractal models for the description of rock surface roughness, *J. Geophys. Res.*, *93*, 415–424, 1991.

Prejean, S. G., and W. L. Ellsworth, Observations of earthquake source parameters and attenuation at 2 km depth in the Long Valley Caldera, Eastern California, *Bull. Seismol. Soc. Am.*, *91*, 165–177, 2001.

Reynolds, O., On the theory of lubrication and its application to Mr. Beauchamp Tower's experiments, including an experimental determination of the viscosity of olive oil, *Philos. Trans. R. Soc. London*, *177*, 157–234, 1886.

Rumble, D., Water circulation in metamorphism, *J. Geophys. Res.*, *99*, 15,499–15,502, 1994.

Sato, T., and T. Hirasawa, Body wave spectra from propagating shear cracks, *J. Phys. Earth*, *21*, 415–431, 1973.

Scholz, C. H., *The Mechanics of Earthquakes and Faulting*, Cambridge Univ. Press, New York, 1990.

Sengers, J., and J. Watson, Improved international formulations for the viscosity and thermal-conductivity of water substance, *J. Phys. Chem. Ref. Data*, *15*, 1291–1314, 1986.

Sibson, R., Interactions between temperature and pore-fluid pressure during earthquake faulting and a mechanism for partial or total stress relief, *Nature Phys. Sci.*, *243*, 66–68, 1973.

Sibson, R., Thickness of the seismogenic slip zone: Constraints from field geology, *Eos Trans. AGU*, *80*(46), Fall Meet. Suppl., F727, 1999.

Singh, S., and M. Ordaz, Seismic energy release in mexican subduction zone earthquakes, *Bull. Seismol. Soc. Am.*, *84*, 1533–1550, 1994.

Sommerfeld, A., *Mechanics of Deformable Bodies*, Academic, San Diego, Calif., 1950.

Spikes, H., Mixed lubrication–an overview, *Lubric. Sci.*, *9*, 221–253, 1997.

Spray, J. G., Viscosity determinations of some frictionally generated silicate melts: Implications for fault zone rheology at high strain rates, *J. Geophys. Res.*, *98*, 8053–8068, 1993.

Szeri, A. Z., *Fluid Film Lubrication: Theory & Design*, Cambridge Univ. Press, New York, 1998.

Timoshenko, S., and J. Goodier, *Theory of Elasticity*, McGraw-Hill, NewYork, 1970.

Venkataraman, A., L. Rivera, and H. Kanamori, Radiated energy from the october 16, 1999 hector mine earthquake: regional and teleseismic estimates, *Eos Trans. AGU*, *81*(48), Fall Meet. Suppl., F843, 2000.

Wald, D. J., and T. H. Heaton, Spatial and temporal distribution of slip for the 1992 Landers, California, earthquake, *Bull. Seismol. Soc. Am.*, *84*, 668–691, 1994.

Wald, D. J., H. Heaton, Thomas, and K. Hudnut, The slip history of the 1994 Northridge, California, earthquake determined from strong-motion, teleseismic, GPS, and leveling data, *Bull. Seismol. Soc. Am.*, *86*, S49–S70, 1996.

E. E. Brodsky, Department of Earth and Planetary Sciences, McCone Hall, University of California Berkeley, Berkeley, CA 94720, USA. (brodsky@gps.caltech.edu)

H. Kanamori, Seismological Laboratory, MC 252-21, California Institute of Technology, Pasadena, CA 91125, USA. (hiroo@gps.caltech.edu)

(Received May 12, 2000; revised December 1, 2000; accepted March 26, 2001.)